NANO LETTERS
Cite This: Nano Lett. 2018, 18, 1530−1534
Letter
pubs.acs.org/NanoLett

Reversibly Bound Kinesin-1 Motor Proteins Propelling Microtubules Demonstrate Dynamic Recruitment of Active Building Blocks

Amy Tsui-Chi Lam, Stanislav Tsitkov, Yifei Zhang, and Henry Hess*

Department of Biomedical Engineering, Columbia University, New York City, New York 10027, United States

Supporting Information

ABSTRACT: Biological materials and systems often dynamically self-assemble and disassemble, forming temporary structures as needed and allowing for dynamic responses to stimuli and changing environmental conditions. However, this dynamic interplay of localized component recruitment and release has been difficult to achieve in artificial molecular-scale systems, which are usually designed to have long-lasting, stable bonds. Here, we report the experimental realization of a molecular-scale system that dynamically assembles and disassembles its building blocks while retaining functionality. In our system, filaments (microtubules) recruit biomolecular motors (kinesins) to a surface engineered to allow for the reversible binding of the kinesin-1 motors. These recruited motors work to propel the cytoskeletal filaments along the surface. After the microtubules leave the motors behind, the trail of motors disassembles, releasing the motors back into solution. Engineering such dynamic systems may allow us to create materials that mimic the way in which biological systems achieve self-healing and adaptation.

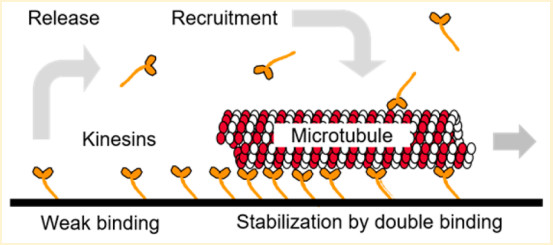

KEYWORDS: *Kinesin, microtubule, reversibility, self-organization*

Biological systems often manifest self-organized, dynamic behaviors.[1,2] For example, stress fibers and filipodia are temporarily formed from molecular building blocks to support cellular motility.[3] Similarly, social insects dynamically recruit group members for the performance of localized tasks, e.g., foraging.[4] However, engineered systems and materials on the molecular scale are usually designed to have specific and strong interactions to facilitate correct and durable associations between building blocks.[5−7] Thus, creating dynamically self-assembling structures has been a long-standing challenge. Breaking and reforming bonds between components often requires a large change in the environmental conditions, typically implemented through some external mechanism, e.g., by heating and cooling the system[8] or manipulating electromagnetic fields.[7,9−11] These mechanisms will usually reset the system rather than allow for gradual adaptation to the environment.[2,12]

Designing a system in which the components are bonded to one another reversibly during normal operation requires the bonds between components to be tailored to balance the strength required for stability with weakness required for spontaneous dissociation. Such systems have been studied theoretically[2,13] and achieved at the macro- and mesoscale, e.g., in defect-tolerant computing systems,[14] assembling and reorganizing swarms of robots,[15] and particles within electric and magnetic fields.[7,9] However, this has been difficult to realize at the molecular scale. Creating molecular-scale systems in which components continually assemble and reorganize into structures autonomously would enable the exploration of a wide range of dynamic behaviors.[13]

Here, we report the realization of a dynamically assembling and disassembling system in which molecular shuttles (microtubule filaments) construct and are propelled by tracks of assembled kinesin-1 motors, hereafter referred to as "kinesin". These kinesin tracks are temporarily left behind by the shuttle and are released back into solution over time with the possibility of being rerecruited into another trail (Figure 1). In contrast to traditional molecular shuttle systems, the interactions between the surface and the kinesin motors were engineered to be weak and temporary but stable enough to allow for the forward motion of the molecular shuttles (Supporting Information section 1). In this system, a population of kinesin motors are kept free in solution and can bind reversibly to microtubules with rate constants k_1 and k_{-1} (Figure 1 and Supporting Information sections 2 and 3). The microtubule-bound motors may then bind to the surface at rate k_2 converting into motors bound to both surface and microtubule. Although the motors are bound to the surface reversibly, the presence of the microtubule, which is held near the surface by other motors, in turn holds the kinesin motors near the surface as well, allowing the motors to reattach to the surface should they detach from the surface. Thus, the microtubules act as a stabilizer for the processive kinesin motors, holding them in place if they detach from the surface, and allowing them to quickly rebind.[16] The microtubule is propelled forward by the motors attached to both the filament and the surface, and leaves a trail of surface-bound motors

Received: December 20, 2017
Revised: January 8, 2018
Published: January 10, 2018

DOI: 10.1021/acs.nanolett.7b05361
Nano Lett. 2018, 18, 1530−1534

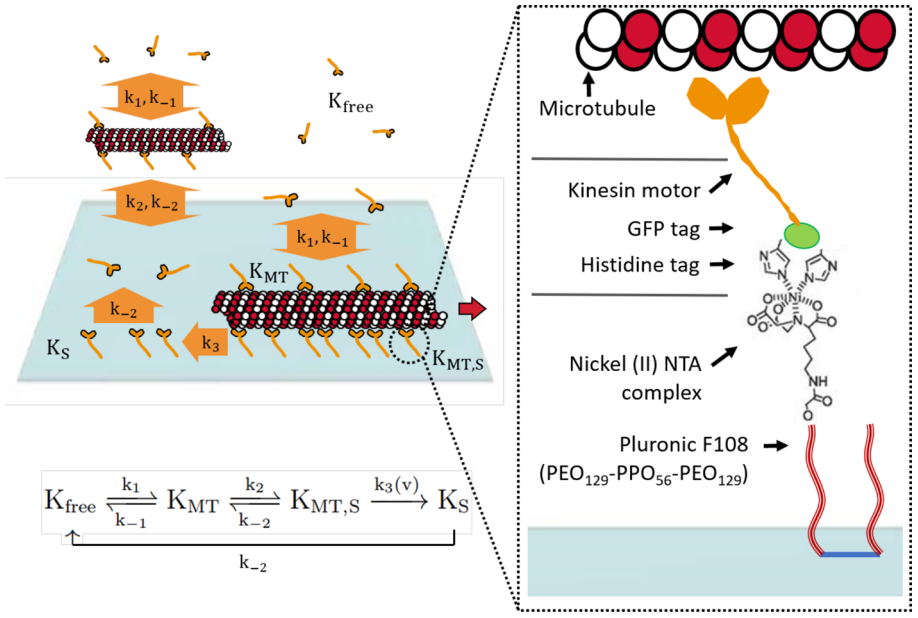

Figure 1. Schematic of our dynamic, self-organized molecular-scale system: In our modified microtubule-kinesin gliding assay, the surface is engineered to bind kinesin motors only transiently. Microtubules recruit kinesins from solution and place them on the surface according to the reaction scheme shown. To obtain reversible binding, the surface is coated with Pluronic-F108 co-polymer functionalized with Ni-NTA. Ni-NTA, in turn, interacts weakly with the histidine-tagged GFP-kinesin fusion protein (right panel).

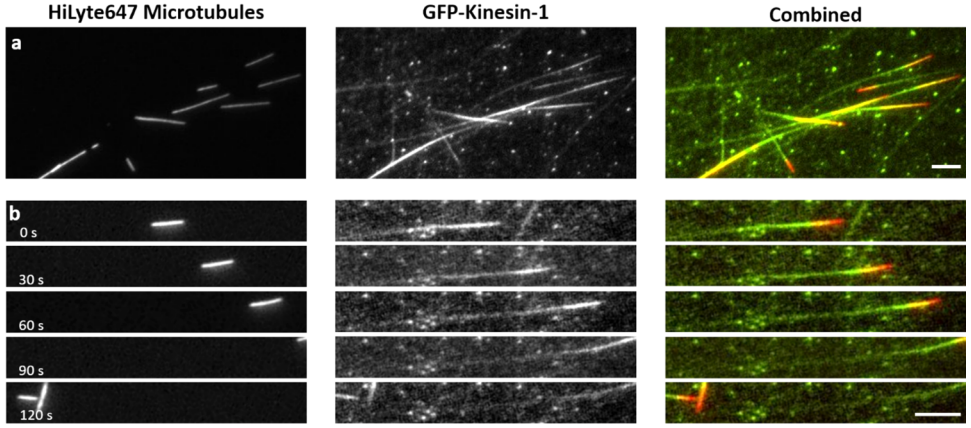

Figure 2. Fluorescence microscopy images of a kinesin trail being assembled and disassembled. (a) HiLyte647-labeled microtubules (red) laden with GFP-kinesin motors (green) are propelled along the surface. As a microtubule moves, it leaves a kinesin trail behind. For this assay, 10 μM ATP and 10 nM kinesin in BRB20 (low-salt) buffer were used. (b) Time-lapse images of a kinesin trail being deposited and then disappearing within 2 min (see also Supporting Information Movie 1). Left panels are the 647 nm channel (HiLyte647 microtubules); center panels are the 488 nm channels (GFP-kinesin); right panels are the two channels overlaid (488 nm channel in green and 647 nm channel in red). Scale bars: 5 μm.

behind at a gliding velocity-dependent rate, k_3. Motors that are bound only to the surface detach with rate constant k_{-2} and are recycled in the solution. This approach requires that k_{-2} should be as large as possible to permit rapid turnover while still being smaller than k_{-1}, so that unbinding from the surface does not interfere with force generation (Supporting Information sections 1 and 3).

Results and Discussion. We constructed this weakly binding surface by silanizing a glass coverslip with dimethyldichlorosilane and then coating it with Pluronic-F108 functionalized with nitrilotriacetic acid (NTA)[17] in 50 mM nickel(II) sulfate. The NTA forms a chelation complex with the nickel ions to which the histidine (His)-tagged GFP-kinesin motors reversibly bind (Figure 1) with an experimentally determined desorption rate constant, k_{-2}, on the order of 0.1 s^{-1} (Supporting Information sections 2 and 3). Our values for the unbinding rate for kinesin from the Ni–NTA complex compare well with the literature: Kienberger et al. studied the NTA-His_6 bond using force spectroscopy, extrapolating an off-rate at zero force of 0.07 s^{-1}.[18] Lata et al. subsequently measured an unbinding rate of a His_6 tag from a single NTA group of 1.8 s^{-1} and from two NTA groups (bis-NTA) of 0.025 s^{-1}.[19] Finally, Verbelen et al. reexamined the force spectroscopy of the NTA-His_6 bond and found that a single His_6 tag can bind up to 3 NTA groups (in accordance with Lata et al.), with a distance to the activation barrier of 0.19 nm, again extrapolating an off-rate of 0.07 s^{-1} for a His_6 tag bound to a single NTA.[20] The activation barrier indicates that the His_6–NTA bond is much less force-sensitive than the kinesin-microtubule bond.

Nonspecific binding of the GFP-kinesin motors to a Pluronic-NTA coated surface in the absence of nickel ions in solution is negligible (Supporting Information section 4).

DOI: 10.1021/acs.nanolett.7b05361
Nano Lett. 2018, 18, 1530–1534

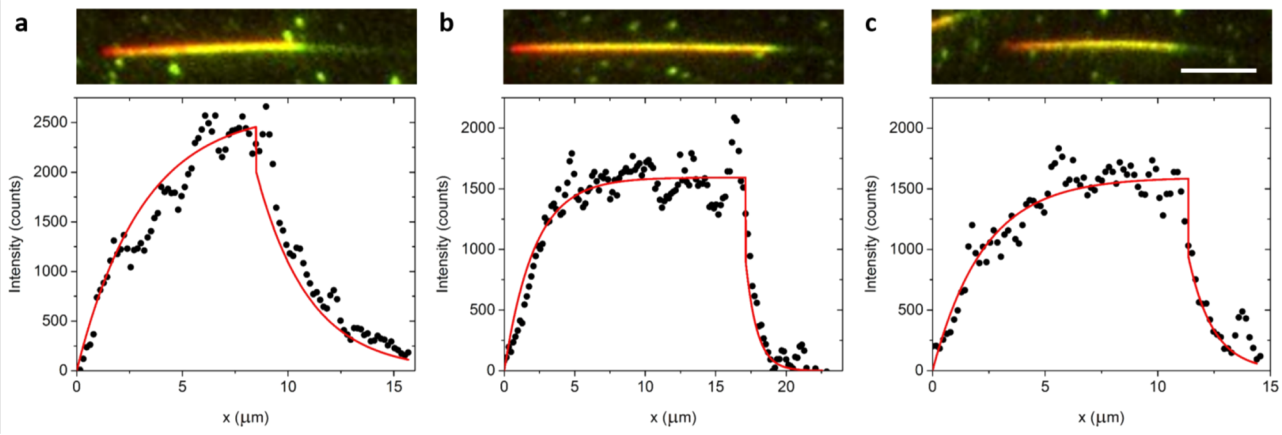

Figure 3. Kinesin trails are assembled by the microtubule and disassemble behind it. (a–c) The 488 nm channel (kinesin) intensities are fit to a model described in supplementary sections 2 and 3 and rate constants are derived. A total of 10 μM ATP and 10 nM kinesin in BRB20 (low-salt) buffer were used. Scale bar: 5 μm.

Furthermore, adding imidazole, a competitive inhibitor to histidine–NTA bond formation, interferes with kinesin binding to the surface (Supporting Information section 4). This demonstrates that the GFP-kinesin does indeed attach specifically via NTA–His_6 binding.

HiLyte647-labeled microtubules and the GFP-kinesin are imaged via fluorescence microscopy by alternating between the two excitation channels. Microtubules are observed to recruit GFP-kinesin from the solution, bind to the surface, and be propelled forward by the kinesin. As they move, a trail of GFP-kinesin is left behind that desorbs within a minute (Figure 2 and Supporting Information Movie 1). In the absence of nickel ions, the NTA groups cannot form the Ni-NTA chelation complex to which the histidine-tagged GFP-kinesins bind. The microtubules are still able to collect kinesin from the solution and diffuse freely within the flow cell, but they too do not bind to the surface (Supporting Information section 4).

The analysis of the GFP-kinesin fluorescence intensity along a microtubule and its trail yields insights into the kinetics of the system (Figure 3). The capture of GFP-kinesin leads initially to a linear increase in the GFP-kinesin fluorescence intensity that saturates within a few micrometers along the microtubule. Because there is only a minor drop in the GFP-kinesin fluorescence directly behind the end of the microtubule, the majority of GFP-kinesins must be adsorbed to both the microtubule and the surface. The GFP-kinesin left behind by the microtubule dissociates from the surface with first-order reaction kinetics. A kinetic model (Figure 1) describing the motor density along the microtubule as a function of time can be used to determine the attachment and detachment rates (k_1 and k_{-1}, respectively) of the GFP-kinesin to the microtubule and the surface (k_2 and k_{-2}) from the fits. We find (Supporting Information section 3) that GFP-kinesins bind from solution to the microtubule with a rate of $k_1 = 0.26 \pm 0.08$ nM^{-1} μm^{-1} s^{-1} for BRB80 buffer and $k_1 = 0.65 \pm 0.15$ nM^{-1} μm^{-1} s^{-1} for BRB20 buffer. Most of the GFP-kinesins bound to the microtubule are able to reach the surface. Once bound, GFP-kinesins can return to the solution with a rate $k_{-1} = v/L$, where v is the stepping velocity (assumed to be equal to the gliding velocity), and $L = 0.86 \pm 0.07$ μm is the run length at zero force for ATP concentrations above 3 μM taken from ref 21. GFP-kinesins held by the microtubule can also attach to the surface, and we find the rate of kinesin-surface attachment ($k_2 >$ 0.3 s^{-1} for BRB80 buffer and $k_2 > 0.5$ s^{-1} for BRB20) to be of similar magnitude as the rate of unbinding from the microtubule. We determine that GFP-kinesins unbind from the surface at a rate $k_{-2} = 0.07 \pm 0.02$ s^{-1} for BRB80 ($k_{-2} = 0.16 \pm 0.01$ s^{-1} for BRB20). These rates are in good agreement with previous measurements of similar systems,[22−24] as described in Supporting Information section 3.

The rate of GFP-kinesin binding to the surface (k_2) in the absence of a microtubule can be obtained using the above-determined unbinding rate (k_{-2}) in conjunction with an experiment determining the binding equilibrium constant (Supporting Information sections 2 and 3) and is found to be $k_2 = 0.02 \pm 0.01$ μm^{-2} nM^{-1} s^{-1}. Because the microtubule can bind to surface-adhered motors along a swath with a width w of less than 100 nm,[16] the rate at which the surface binds motors in the swath accessible to the microtubule (given by $w \cdot k_2$) is 2 orders of magnitude lower than the rate at which the microtubule recruits motors from solution (k_1). This matches the observation (Figures 2 and 3) that the majority of GFP-kinesins supporting microtubule gliding must be recruited by the microtubule itself rather than being already present on the surface.

Stable microtubule gliding requires a certain minimum density ρ_{min} of motors along the microtubule,[25,26] which we determined to be $\rho_{min} = 2$ μm^{-1} for our system (Supporting Information section 5). If we assume that this minimum kinesin density must be present already in the moment of microtubule landing (microtubules appear to be uniformly covered with kinesin in the moment of landing), the velocity dependence of the kinesin unbinding from the microtubule ($k_{-1} = v/L$) introduces a maximum velocity at which gliding is sustained for a given kinesin concentration (Supporting Information section 3):

$$v_{max} = \frac{k_1 L c}{2\rho_{min}} \quad (1)$$

where v_{max} is the maximum sustainable velocity, k_1 is the rate of kinesin capture by microtubules, L is the run-length of kinesin on the microtubule, and c is the concentration of kinesin in solution.

The prediction of eq 1 is confirmed by our experiments. We varied ATP concentrations to achieve different motor velocities and observed stable gliding only below the threshold defined by

DOI: 10.1021/acs.nanolett.7b05361
Nano Lett. 2018, 18, 1530−1534

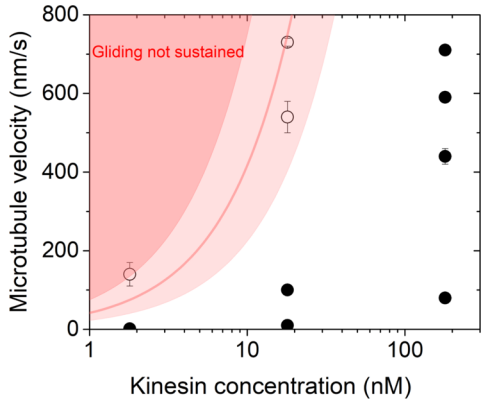

Figure 4. Phase diagram showing the region of sustained microtubule gliding as a function of gliding velocity and kinesin concentration (in BRB80 buffer). Filled circles indicate combinations of velocity and kinesin concentration at which motility was sustained; open circles indicate velocities at which motility was not sustained (i.e., the microtubule detached from the surface). Microtubule gliding velocities are varied by varying the concentration of ATP from 0.1 μM to 10 mM. The model predicts the upper boundary (red line) for the microtubule velocity and kinesin concentration combinations showing sustained gliding. The model uncertainty is indicated by the lightly colored region (see also Supporting Information section 6 and Supporting Information Movies 2–4).

eq 1 (Figure 4, Supporting Information section 6, and Supporting Information Movies 2–4). In contrast, in a traditional shuttle system, in which the motors are permanently attached to the surface, as long as a minimum motor density covers the surface, the filaments can be propelled at the maximum gliding speed of about 900 nm/s.[27] Thus, there is a trade-off in our system between using fewer resources (a lower kinesin concentration) and the maximum speed of shuttle propulsion. We also find that at high kinesin concentrations, motility is maintained for over 10 h, which is comparable to a traditional gliding assay. However, at lower kinesin concentrations, microtubule densities drop over time (Supporting Information section 6).

Kinesin motors are poorly utilized when they are permanently attached to a surface, because only a small fraction of motors comes into contact with a microtubule. On a weakly binding surface, a much larger fraction of surface-adhered motors is in contact with a microtubule, but at the same time, a large pool of kinesin motors is free in solution. Under our experimental conditions, the overall utilization of kinesin motors is equal or better for the weakly binding surface compared to the permanently binding surface (Supporting Information sections 7 and 8), although the gliding velocity may be limited as shown in Figure 4. Further improvement to resource allocation can be achieved by decreasing the height of the flow cell (Supporting Information section 7).

Conclusions. Our work demonstrates a molecular-scale system in which weak connections are key to the dynamic organization of force-producing building blocks. Dynamic molecular systems of this type may offer advantages in applications in which system plasticity or healing is desired. For example, a system's ability to continually assemble itself may enable it to adapt to load by recruiting more or fewer force-generating components as needed. Such a system would be able to mold itself to its environment in a way similar to biological tissues and systems (e.g., muscle). This also raises the broader question of reliability engineering for molecular-scale systems, in which not only failure events but also replacement events are stochastic in nature.[28]

Methods. Microtubules were polymerized by reconstituting 20 μg of HiLyte647-labeled lyophilized tubulin (TL670M, Lot 017 from Cytoskeleton Inc., Denver, CO) in 6.25 μL of polymerization buffer (BRB80 buffer and 4 mM $MgCl_2$, 1 mM GTP, 5% dimethyl sulfoxide) and incubating at 37 °C for 45 min. BRB80 buffer contains 80 mM piperazine-*N*,*N*′-bis(2-ethanesulfonic acid), 1 mM $MgCl_2$, and 1 mM ethylene glycol tetraacetic acid at a pH of 6.9 (adjusted with KOH). The microtubules were then stabilized by diluting them 100× into BRB80 buffer with 10 μM paclitaxel (Sigma, Saint Louis, MO).

A kinesin construct containing the first 430 amino acids of rat kinesin heavy chain fused to eGFP and a C-terminal His-tag at the tail domain (rkin430eGFP)[29] was expressed in *Escherichia coli* and purified using a Ni–NTA column (prepared by G. Bachand at the Center for Integrated Nanotechnologies at Sandia National Laboratories). The concentration of the GFP-kinesin stock solution was 1.8 ± 0.3 μM.

Flow cells were constructed using two coverslips held together with double-sided tape.[30] All coverslips were first washed with ethanol and then Milli-Q water before being sonicated in Milli-Q water for 5 min. They were then oven-dried and UV/ozone treated on both sides for 15 min (UV Ozone Procleaner, BioForce Nanosciences). The coverslips were again sonicated in Milli-Q water for 5 min before drying.

To coat the surface with Pluronic-F108, the cleaned coverslips were immersed in 5% dimethyldichlorosilane in toluene (Sigma, Saint Louis, MO) for 15 s before being washed twice in toluene and three times in methanol. The coverslips were dried with nitrogen. These treated coverslips were assembled into a flow cell. A solution of 2 mg/mL Pluronic F108-NTA (a gift from Dr. Jennifer Neff, AllVivo Vascular, Lake Forest, CA) in 50 mM nickel(II) sulfate (Sigma, Saint Louis, MO) was first flowed into the flow cell. The pluronic NTA was allowed to adsorb for 5 min before being washed out three times with buffer solution, either BRB80 or BRB20 (20 mM piperazine-*N*,*N*′-bis(2-ethanesulfonic acid), 1 mM $MgCl_2$, and 1 mM ethylene glycol tetraacetic acid, pH 6.9 with KOH). Next, a solution containing microtubules (3.2 μg mL^{-1}), and kinesin and ATP of varying concentrations in 0.5 mg/mL casein (Sigma), 10 μM paclitaxel, an enzymatic antifade and ATP regenerating system (20 mM D-glucose, 20 μg mL^{-1} glucose oxidase, 8 μg mL^{-1} catalase, 10 mM dithiothreitol, 2 mM creatine phosphate, and 2 units L^{-1} creatine phosphokinase in BRB80 or BRB20 buffer), was flowed in and incubated for 10 min before being exchanged for a solution containing a matching concentration of kinesin, ATP, paclitaxel, and antifade system (but without microtubules). The edges of the flow cell were sealed with vacuum grease to prevent evaporation.

Both the microtubules and kinesin were imaged using an objective-type total internal reflection fluorescence setup on an Eclipse Ti microscope (Nikon Instruments, Melville, NY) with a 100×/1.49 NA objective lens (Nikon Instruments, Melville, NY) using a 650 nm laser and a 480 nm laser for the imaging of microtubules and kinesin, respectively. Images were taken with an iXON DU897 Ultra EMCCD Camera (Andor Technology, South Windsor, CT) once every 10 s (exposure time of 50 ms for both channels) for as long as motility was noted. All experiments were performed at ~24 °C.

DOI: 10.1021/acs.nanolett.7b05361
Nano Lett. 2018, 18, 1530–1534

■ ASSOCIATED CONTENT

Supporting Information

The Supporting Information is available free of charge on the ACS Publications website at DOI: 10.1021/acs.nanolett.7b05361.

Additional details on the impact of weak binding on force generation and efficiency, analysis of fluorescence signals, control experiments, determination of the minimum microtubule kinesin density for sustained gliding, microtubule movement, resource allocation, and theoretical comparison. (PDF)

Time-lapse movie of an experimental assay run with 10 nM kinesin and 10 microM ATP in BRB20 buffer. A microtubule (red) assembles and is propelled along the surface by kinesin-1 motors (green). As the microtubule moves, it leaves a kinesin trail behind, which desorbs from the surface over the course of two minutes. (AVI)

Time-lapse movie of an experimental assay run with 180 nM kinesin and 1 mM ATP in BRB80 buffer. Microtubules move at the maximum sustainable velocity observed (710 ± 10 nm/s) for this kinesin concentration. (AVI)

Time-lapse movie of an experimental assay run with 18 nM kinesin and 10 microM ATP in BRB80 buffer. Microtubules move at the maximum sustainable velocity observed (110 ± 3 nm/s) for this kinesin concentration. (AVI)

Time-lapse movie of an experimental assay run with 1.8 nM kinesin and 0.1 microM ATP in BRB80 buffer. Microtubules move at the maximum sustainable velocity observed (1.6 ± 0.1 nm/s) for this kinesin concentration. (AVI)

■ AUTHOR INFORMATION

Corresponding Author

*E-mail: hh2374@columbia.edu.

ORCID

Yifei Zhang: 0000-0002-0014-611X

Henry Hess: 0000-0002-5617-606X

Author Contributions

A.T.L., S.T., Y.Z., and H.H. designed and conceived the experiments. A.T.L., S.T., and Y.Z. performed the experiments and analysis. A.T.L. and H.H. wrote the paper.

Funding

The authors acknowledge financial support from the US Army Research Office under grant no. W911NF-13-1-0390.

Notes

The authors declare no competing financial interest.

■ ACKNOWLEDGMENTS

The authors thank G. Bachand for providing the GFP-kinesin protein. This work was performed, in part, at the Center for Integrated Nanotechnologies, an Office of Science User Facility operated for the US Department of Energy (DOE) Office of Science by Los Alamos National Laboratory (contract no. DE-AC52-06NA25396) and Sandia National Laboratories (contract no. 97 DE-AC04-94AL85000). The authors thank Dr. Jennifer Neff and AllVivo Vascular for their gift of Pluronic-F108 functionalized with NTA.

■ REFERENCES

(1) Whitesides, G. M.; Grzybowski, B. *Science* **2002**, *295*, 2418−2421.
(2) Fialkowski, M.; Bishop, K. J. M.; Klajn, R.; Smoukov, S. K.; Campbell, C. J.; Grzybowski, B. A. *J. Phys. Chem. B* **2006**, *110*, 2482−2496.
(3) Nemethova, M.; Auinger, S.; Small, J. V. *J. Cell Biol.* **2008**, *180*, 1233−1244.
(4) Bonabeau, E.; Dorigo, M.; Theraulaz, G. *Nature* **2000**, *406*, 39−42.
(5) Whitesides, G. M.; Boncheva, M. *Proc. Natl. Acad. Sci. U. S. A.* **2002**, *99*, 4769−4774.
(6) Ringler, P.; Schulz, G. E. *Science* **2003**, *302*, 106−109.
(7) Boncheva, M.; Whitesides, G. M. *Angew. Chem., Int. Ed.* **2003**, *42*, 2644−2647.
(8) Plaisted, T. A.; Nemat-Nasser, S. *Acta Mater.* **2007**, *55*, 5684−5696.
(9) Grzegorczyk, T. M.; Rohner, J.; Fournier, J.-M. *Phys. Rev. Lett.* **2014**, *112*, 023902.
(10) Ghosh, B.; Urban, M. W. *Science* **2009**, *323*, 1458−1460.
(11) Burnworth, M.; Tang, L.; Kumpfer, J. R.; Duncan, A. J.; Beyer, F. L.; Fiore, G. L.; Rowan, S. J.; Weder, C. *Nature* **2011**, *472*, 334−337.
(12) Hermans, T. M.; Frauenrath, H.; Stellacci, F. *Science* **2013**, *341*, 243−244.
(13) England, J. L. *Nat. Nanotechnol.* **2015**, *10*, 919−923.
(14) Heath, J. R.; Kuekes, P. J.; Snider, G. S.; Williams, R. S. *Science* **1998**, *280*, 1716−1721.
(15) Rubenstein, M.; Cornejo, A.; Nagpal, R. *Science* **2014**, *345*, 795−799.
(16) Palacci, H.; Idan, O.; Armstrong, M. J.; Agarwal, A.; Nitta, T.; Hess, H. *Langmuir* **2016**, *32*, 7943−7950.
(17) deCastro, M. J.; Ho, C. H.; Stewart, R. J. *Biochemistry* **1999**, *38*, 5076−5081.
(18) Kienberger, F.; Kada, G.; Gruber, H. J.; Pastushenko, V. P.; Riener, C.; Trieb, M.; Knaus, H. G.; Schindler, H.; Hinterdorfer, P. *Single Mol.* **2000**, *1*, 59−65.
(19) Lata, S.; Reichel, A.; Brock, R.; Tampé, R.; Piehler, J. *J. Am. Chem. Soc.* **2005**, *127*, 10205−10215.
(20) Verbelen, C.; Gruber, H. J.; Dufrêne, Y. F. *J. Mol. Recognit.* **2007**, *20*, 490−494.
(21) Schnitzer, M. J.; Visscher, K.; Block, S. M. *Nat. Cell Biol.* **2000**, *2*, 718−723.
(22) Varga, V.; Leduc, C.; Bormuth, V.; Diez, S.; Howard, J. *Cell* **2009**, *138*, 1174−1183.
(23) Roos, W. H.; Campàs, O.; Montel, F.; Woehlke, G.; Spatz, J. P.; Bassereau, P.; Cappello, G. *Phys. Biol.* **2008**, *5*, 046004.
(24) Sheehan, P. E.; Whitman, L. J. *Nano Lett.* **2005**, *5*, 803−807.
(25) Hancock, W. O.; Howard, J. *J. Cell Biol.* **1998**, *140*, 1395−1405.
(26) Fallesen, T. L.; Macosko, J. C.; Holzwarth, G. *Phys. Rev. E* **2011**, *83*, 011918.
(27) Tucker, R.; Saha, A. K.; Katira, P.; Bachand, M.; Bachand, G. D.; Hess, H. *Small* **2009**, *5*, 1279−1282.
(28) Birolini, A. *Reliability Engineering: Theory and Practice*, 6th ed.; Springer: New York, 2010.
(29) Rogers, K. R.; Weiss, S.; Crevel, I.; Brophy, P. J.; Geeves, M.; Cross, R. *EMBO J.* **2001**, *20*, 5101−5113.
(30) Howard, J.; Hunt, A. J.; Baek, S. *Methods Cell Biol.* **1993**, *39*, 137−147.

DOI: 10.1021/acs.nanolett.7b05361
Nano Lett. 2018, 18, 1530−1534